ELSEVIER

Contents lists available at ScienceDirect

Cement and Concrete Composites

journal homepage: www.elsevier.com/locate/cemconcomp





An innovative method for mesoscale modelling of moisture diffusion in concrete

Songsong Meng^{*}, Yifan Li, Iman Hajirasouliha, Giacomo Torelli, Maurizio Guadagnini, Kypros Pilakoutas

Department of Civil and Structural Engineering, The University of Sheffield, S1 3JD, Sheffield, UK

ARTICLE INFO

Keywords:
Pore structure
Brunauer-Skalny-Bodor (BSB) model
Rayleigh-Ritz model
Voronoi diagram
Moisture diffusion
Relative humidity distribution

ABSTRACT

Moisture diffusion influences the durability and long-term performance of concrete and whilst it predominantly occurs via the cement matrix and Interfacial Transition Zone, most existing models consider concrete to be homogeneous. This paper introduces a novel micro-meso model that employs random packing and Voronoi tessellation. Rayleigh-Ritz pore distribution and Brunauer-Skalny-Bodor models are combined to determine the radius and fraction of various pores. The results indicate that relative humidity diffuses faster with increasing temperature, decreasing ambient relative humidity and tortuosity. Ambient relative humidity has a greater influence on diffusion compared to temperature and tortuosity. Numerical and experimental comparisons demonstrate that the proposed methodology effectively captures relative humidity distribution across various scenarios. Furthermore, explicit pore network modelling incorporates key parameters for a more accurate analysis. Integrating the proposed methodology into a fully coupled hygro-mechanical framework can potentially yield more accurate predictions of mechanical behaviour; enhancing the reliability of long-term performance assessments and enabling more durable concrete design.

1. Introduction

Durability is of paramount importance for achieving a long service life in concrete structures. Concrete, inherently porous in nature, is susceptible to moisture transport, enabling aggressive chemical agents to infiltrate and potentially trigger degradation mechanisms [1]. These degradation processes can include chloride penetration [2,3], alkali-silica reaction [4,5], and carbonation [2]. In this context, the transport properties of concrete play a pivotal role in determining its durability [6,7]. Moisture diffusivity, a fundamental property that governs the rate at which moisture propagates through the material, is a key parameter in assessing the resistance of concrete to the deleterious effects of moisture-related phenomena. A robust understanding of moisture diffusivity enables the development of strategies and materials that can mitigate or even prevent these mechanisms of degradation, ultimately extending the service life of concrete structures.

Numerous numerical models have been proposed to predict moisture transport and capillary diffusion in cementitious materials [8–10]. At the mesoscale, diffusivity of the various constituents (phases) of concrete (aggregates, interfacial transition zone (ITZ) and cement matrix) is

required to predict the global moisture transport [11]. For this purpose, theoretical equations for liquid and vapour water based on Darcy's law and Fick's second law are widely employed to express the relationships between moisture diffusion coefficient, water saturation degree and relative humidity (RH) [12-15]. Building upon these principles, Caré and Hervé [16] proposed a mesoscale model to predict the moisture diffusivity of concrete at different volume fractions of coarse aggregate, while Sun et al. [17] developed a multi-phase model that explicitly accounts for the individual phases, including mortar, ITZ and aggregates, as well as a homogenization phase. Huang et al. [18] proposed a multi-scale model that accounts for the pore size distribution and fraction to study moisture diffusion. Moreover, Dehwah and Xi [19] studied the moisture diffusion mechanisms whilst considering different pore sizes by employing molecular, Knudsen and surface diffusions. A generalized self-consistent model was proposed to predict the moisture diffusion in concrete including the influence of coarse aggregates [20]. Nevertheless, these theoretical models still necessitate the use of empirically calibrated moisture diffusion coefficients, based on experimentally determined parameters (e.g. time, RH, distance, temperature), to express their relationship with moisture saturation and RH. Moreover,

E-mail addresses: smeng6@sheffield.ac.uk, mengsongsong_edu@163.com (S. Meng).

^{*} Corresponding author.

the measurement of these parameters is affected by material variability and the precision of the instrumentation [21-24].

Wang and Ueda [25] employed both macro and meso models to derive a theoretical solution for diffusivity by phase, assuming that most diffusion occurs in the mortar and ITZ. However, as 2-D models do not account for porosity and tortuosity of pore structures, these are unlikely to provide accurate predictions for 3-D problems. Furthermore, most models focus on the diffusivity of the phases, treating them as homogeneous, thus making it challenging to understand the impact of pore structure on the diffusion process [18].

In contrast to mesoscale models, microscale models focus on modelling diffusivity based on the microstructure characteristics of the pore structure, which include volume fraction and size distribution. Experimental techniques employed to obtain the pore structure features include: micro imaging generated by X-rays (micro-CT), backscattered electron imaging (BEI), and mercury intrusion porosimetry (MIP). The MIP method can detect a wide range of pore sizes, spanning from 2.5 nm to 10^5 nm. On the other hand, BEL and micro-CT offer two-dimensional and three-dimensional images of pores, along with their spatial distribution. Results show that concrete contains a diverse array of pores, predominantly falling into four categories: (i) C-S-H gel pores (calcium-silicate-hydrate), (ii) small capillaries, (iii) large capillaries and (iv) voids [26].

Zhang and Ye [27] introduced a micro-model to predict moisture diffusion in non-saturated cementitious materials, accounting for different pore radii based on MIP measurements. However, the precision of measured pore radii derived from the MIP method can be compromised by the "ink-bottle" effect [28]. To address this limitation, a cylindrical pore model, coupled with thermodynamic theories, can be employed to more accurately predict moisture diffusion [29–32]. Furthermore, the pore size distribution can be characterized through a multi-Rayleigh-Ritz (R-R) model encompassing various pore types [30]. This pore distribution model uses the pore type fraction and radii to represent the pore density distribution.

Zhang et al. [33] developed a "Lattice Boltzmann" (LB) model for moisture transport to investigate the water-gas diffusion in porous materials. However, they did not account for the gel pores in mortar, despite other studies emphasizing their critical role in moisture diffusion [34–36].

A more accurate prediction of moisture diffusion can thus be achieved by a model that links microstructural features to the diffusion properties of cementitious materials. This can be accomplished by converting the different micro-scale pore types into a homogeneous mesoscale phase. Examples of this include applications of the Maxwell model [37], the differential medium model [38,39], and the self-consistent model [40]. However, these models do not consider coarse aggregates and, hence, are more suited to model mortar rather than concrete.

This paper presents the development of a mesoscopic model for predicting moisture diffusion in concrete based on the Rayleigh-Ritz pore size distribution model. A Voronoi diagram is used to generate a mesh for pores, ITZ surrounding randomly positioned impermeable aggregate, and mortar, resulting in a 2-D concrete mesoscale model. A time-dependent model is employed to account for non-steady state diffusion and predict the moisture transport through the pores and ITZ. The proposed model is validated against experimental results. Based on this model, the specific phases of pores and ITZ will contribute towards more precise descriptions of the RH distribution and evolution in concrete. Because of its enhanced predictive capabilities, the model derived herein can be used to study multi-phase coupled problems, such as thermo-hygral, hygro-mechanical, or thermo-hygro-mechanical problems. Integrating the proposed methodology into existing mechanical frameworks will lead to an increased accuracy in the prediction of the mechanical response of the material, including shrinkage, creep and crack development effects. This in turn will enhance the reliability of long-term performance assessments and facilitate the design of more

durable concrete structures.

2. Geometric properties of mesoscale model

The approach adopted combines the mesoscale geometry and microscale theory to develop the micro-meso (MiMe) model to simulate moisture diffusion. The following sections describe the parameters that are necessary to define the geometry of all concrete constituents e.g., mortar, aggregate, ITZ and pores, and presents the methodology used to develop the mesoscale model.

2.1. Distribution and shapes of aggregate

The Monte Carlo method is used to locate the centroid and diameter of each aggregate and generate their in-plane spatial distribution [41, 42], which is expressed as:

$$\begin{cases} x = x_{\min} + i(x_{\max} - x_{\min}) \\ y = y_{\min} + j(y_{\max} - y_{\min}) \end{cases}$$
 (1)

where, x_{\min} , x_{\max} , y_{\min} , y_{\max} are the lower and upper limit of the concrete plane in x and y directions, respectively; and i and j are random numbers sampled between 0 and 1.

Specific rules regarding the judgement of interaction between aggregates are imposed to avoid overlap of individual aggregates and ensure that each aggregate is located within the boundaries of the specimen, which are expressed as:

$$\sqrt{(x-x')^2+(y-y')^2} \ge \frac{(d+d')}{2}$$
 (2)

where, x', y' and d' are the coordinates of previous aggregates and diameters, respectively.

Based on the mix design (in kg/m 3 : water 168, OPC 420, river sand 718 and crushed granite aggregate 1127; and the density of the aggregate (2700 kg/m 3) a volume ratio of 42 % aggregate is determined and used to generate the aggregate mesh) [18]. Three size groups are considered based on the grading curve of Mora's sample [43] to create a reasonable aggregate size distribution (4.75–9.5 mm -28.4 %, 9.5–12.5 mm -63.6 % and 12.5–16 mm 8 %).

Polygonal aggregates with a diameter ranging from 4.75 to 16 mm are created by employing the Fuller distribution [44] to generate the number of edges and angles of polygon (α). A typical two-dimensional random polygon aggregate model is shown in Fig. 1.

2.2. Geometric properties of the ITZ

Although the ITZ enhances the pore network connectivity, it also affects the overall tortuosity and complicates the diffusion process in ways that cannot be easily quantified. As a result, diffusion within the ITZ is often treated similarly to diffusion within the pore network [45].

The diffusion properties of the ITZ are dominated by total pore volume within this zone. Moisture transport is assumed to occur exclusively within the ITZ, which can be visualised as the zone surrounding the aggregates with a thickness "t" (see Fig. 2), and does not occur through the interfaces with mortar and aggregates. The thickness of the ITZ is generally considered to be of the order of 0.05 mm [18], hence this value is adopted in the present study.

2.3. Mortar pore structure

In this study the bulk of the mortar matrix is considered to be impermeable, akin to aggregates. Therefore, the diffusion process occurs exclusively through a network of interconnected pores, capillaries, and ITZ. As continuous interconnectivity of the pore structure is assumed, the formation of percolating paths is inherent to this model and independent of aggregate size and content.

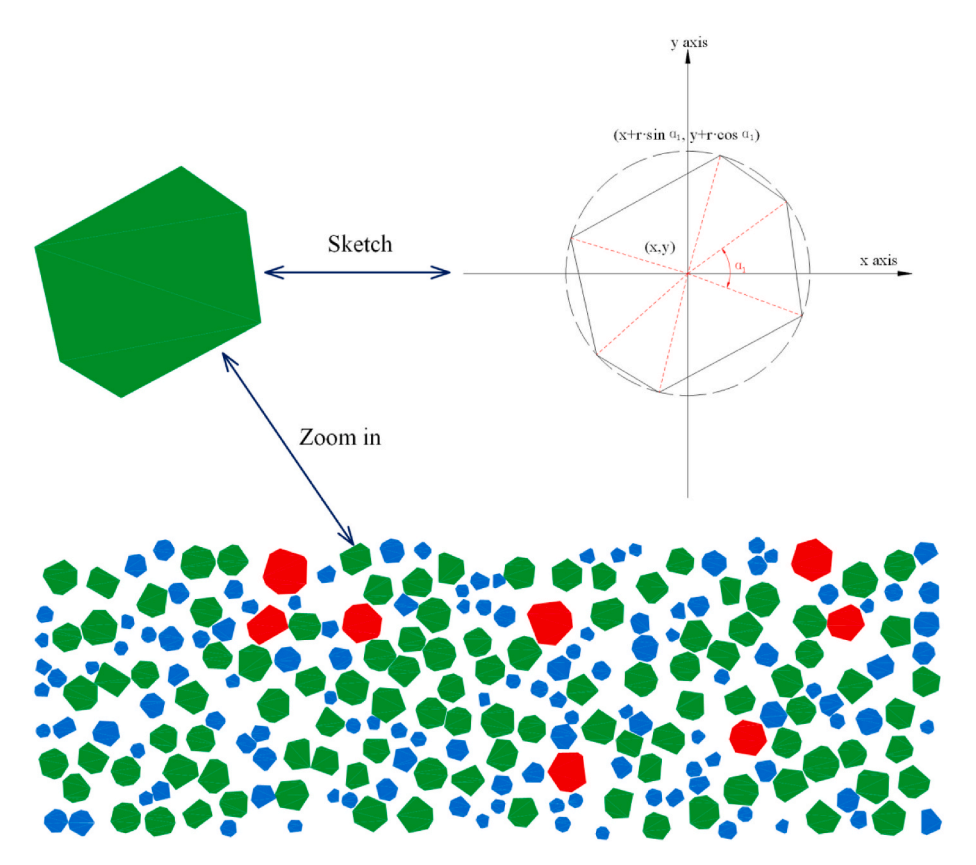


Fig. 1. 2-D random distribution of polygonal aggregates.

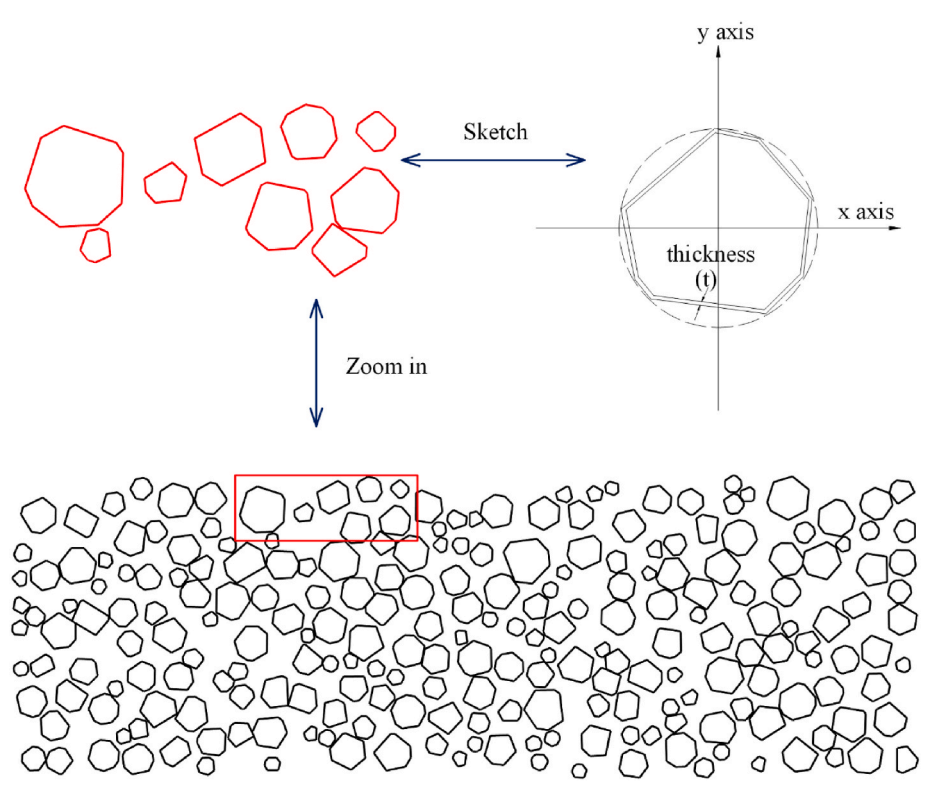


Fig. 2. 2-D random distribution of polygonal ITZ.

To create the capillary structure, the Voronoi tessellation method for polygonal geometrical elements [46] is adopted. This method generates an array of randomly allocated nodes, located at the centroid of the

Voronoi regions within the mortar. These nodes are interconnected via equidistant segments that either intersect or meet at the ITZ, as depicted in Fig. 3(a) and (b). The nominal width of these capillary segments is set

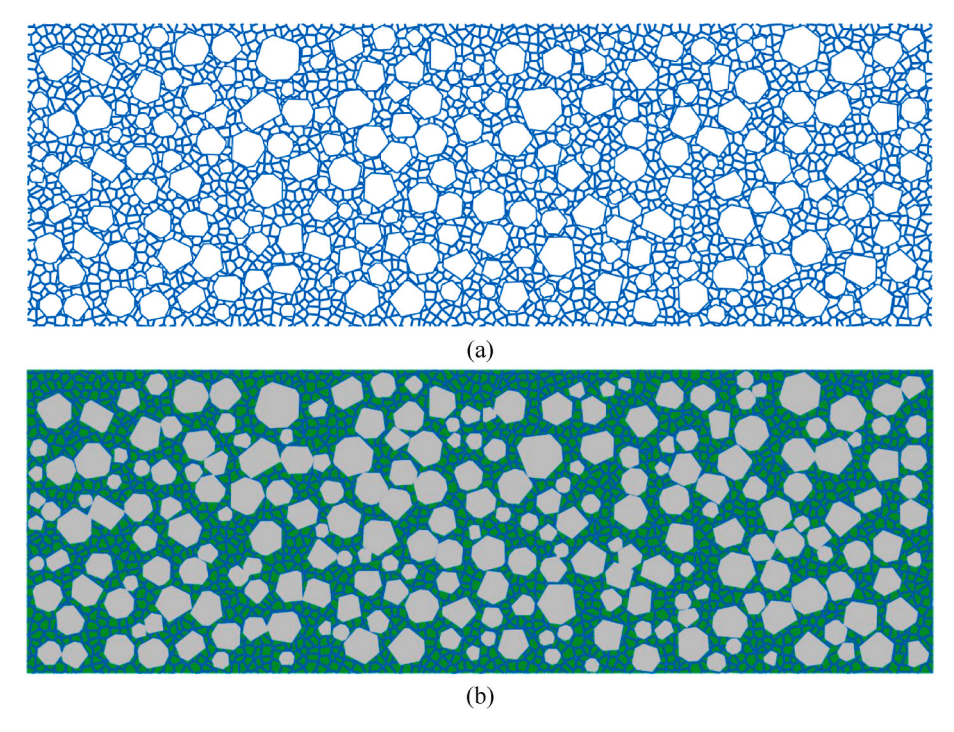


Fig. 3. (a) capillary structure, and (b) overall network.

at 0.3 mm and the total area of the capillary network is determined on the experimentally derived porosity from MIP or other methods.

3. Theoretical framework for diffusion through capillary structure

Moisture transport in concrete is driven by flow potential, resulting in both diffusion (for vapour water) and permeation (for liquid water) that lead to desorption and adsorption [47–49]. Desorption occurs when concrete is exposed to an environment with relatively low RH. Liquid water diffuses due to capillary stress, whilst vapour water diffuses through pores that are partially unoccupied (by liquid) due to gas pressure differential.

According to the extended Darcy's equation, the flow rate of liquid water $(J_L \text{ (kg·m}^{-2}\text{s}^{-1}))$ can be expressed as follows:

$$J_L = -K_L(h)\frac{\partial p_c}{\partial x} \tag{3}$$

where K_L (s) is the diffusion coefficient of liquid water as a function of h (RH %), p_G (Pa) is the capillary pressure.

The relationship between RH and capillary stress is obtained using Kelvin's equation and expressed as follows:

$$p_c = -\frac{\rho_L RT \ln h}{M_w} \tag{4}$$

where M_w is the mass of water per unit molecule (kg/mol), ρ_L is the density of liquid water (kg/m³), R is the universal gas constant (J·K⁻¹mol⁻¹), and T is the temperature at the point under consideration (K)

Fick's law is employed to express the flux balance of water mass in the diffusion process of vapour:

$$J_V = -K_V(h)\frac{\partial p_v}{\partial x} \tag{5}$$

where J_V is the diffusion flux of water vapour (kg·m⁻²s⁻¹), K_V is the diffusion coefficient of vapour water varying with h (RH %). The vapour relative humidity is defined as the ratio of vapour to saturated vapour

pressure, $h = p_V/p_{VS}$. Thus, the diffusion of vapour water is expressed as:

$$J_{V} = -K_{V}(h)p_{VS}\frac{\partial h}{\partial x} \tag{6}$$

where J_V is the vapour flow rate (kg·m⁻²s⁻¹), p_V (Pa) is the vapour pressure, p_{VS} (Pa) is the saturated vapour pressure.

For mass balance, the rate of water mass change per unit volume is equal to the difference of moisture flux J across the boundaries of an infinitesimal control volume, which is expressed as:

$$-\frac{\partial w}{\partial t} = \nabla \cdot J \tag{7}$$

By combining Eqs. (3)–(7), the diffusion process including liquid and vapour water is obtained as:

$$\frac{\partial w}{\partial h}\frac{\partial h}{\partial t} = \frac{\partial}{\partial x} \left(K_L \frac{\rho_L RT}{M_W h} \frac{\partial h}{\partial x} + K_V p_{VS} \frac{\partial h}{\partial x} \right) \tag{8}$$

where $\partial w/\partial h$ is the slope of the adsorption or desorption isotherm, w and h are the water content and RH due to moisture diffusion ($w=w_a$ - Δw_s), $h=h_a$ - Δh_s), w_a and h_a are total water content and RH in concrete, Δw_s water loss by hydration process, Δh_s is the RH reduction due to hydration process.

To predict the moisture diffusion, both vapour and liquid permeability of concrete (in Eq. (8)) are needed. These diffusion coefficients, which make up the total diffusivity, depend on the pore radius and distribution and can be obtained using the Rayleigh-Ritz model.

3.1. Rayleigh-Ritz (R-R) distribution for pores

To determine the diffusion coefficients for vapour and liquid water, the diameter and portion of each type of pores needs to be considered. Huang et al. [18] categorize pores based on their diameters into the following types: 1) C-S-H gel pores (smaller than 2.5 nm), 2) small capillaries (from 2.5 nm to 50 nm), 3) large capillaries (from 50 to 105 nm), and 4) voids (greater than 105 nm). However, the larger voids (>105 nm) are normally closed pores that lack connectivity and do not affect the diffusion processes. Moreover, the presence of microcracks

(width more than 1 $\mu m)$ also impacts moisture transport and should be incorporated into the pore size distribution model.

The R-R model can be employed to disaggregate the MIP curve to determine the distribution of each type of pore [50]. The volume fraction of each pore type (ϕ_i) and their representative radius (r) are used to delineate the distribution of each type of pores, expressed as:

$$\phi = \phi_t \sum_{i=1}^{4} \phi_i \left(1 - \exp\left(-\frac{r}{B_i} \right) \right) \tag{9}$$

where ϕ_t is the porosity of concrete, and ϕ_i is the ratio between the porosity of pore type i and the overall porosity. B_i is the pore radius corresponding to the peak of the differential porosity for each pore type on a logarithmic scale.

A random connection of tubular geometry capillaries is adopted to simulate the entire pore structure [50]. Hence, the pore size distribution is related to the density distribution of pores f_d , which is expressed as the derivative of porosity to pore radius r:

$$f_d = \phi_t \sum_{1}^{4} \frac{\phi_i}{B_i} \exp\left(-\frac{r}{B_i}\right) \tag{10}$$

From Fig. 4, the saturation degree S_r can be obtained by integrating the pore specific surface area and the thickness of water molecules along the radial direction:

$$S_r = \frac{1}{\phi} \int_0^{r_c} f_d(r) dr \tag{11}$$

where r_c is the critical radius (i.e. the pore radius below which capillary condensation can occur), and it is given by the sum of the capillary condensate radius r_k and the thickness of the absorbed water on the pore wall t_a , as shown in Fig. 4.

To derive the analytical solution for the R-R model, the well-established water saturation degree solution model by Brunauer-Skalny-Bodor is employed along with the empirical functions introduced by Xi et al. [51] to calculate the saturation degree. The Brunauer-Skalny-Bodor model thus reduces to the two-parameter (C and k) formula shown in Eq. (12):

$$S_r = \frac{h(1-k)[1+(C-1)k]}{(1-kh)[1+(C-1)kh]} \tag{12}$$

The parameters, ϕ_i and B_i , can be obtained by combining Eqs. (10) and (11) and Eq. (12) and implementing a curve-fitting method [52].

3.2. Diffusivity of vapour and liquid water

In concrete, vapour water flows through capillaries into the pores and this movement depends on the flow potential due to difference in RH. The Knudsen's theory is employed to describe the collision between molecules and collision against pore walls of vapour water diffusion.

The vapour water diffusion coefficient, k_V , can be expressed using the following equation [53]:

$$k_V = \frac{D_{va}}{1 + l_m/2r_e} \left(\frac{M_w}{RT}\right) \tag{13}$$

where l_m is the mean free path of water molecules, r_e is the actual radius of the pore, which is equal to r_k (shown in Fig. 4), D_{va} is the permeability of vapour water in air as given below [53]:

$$D_{va} = D_0 \frac{P_0}{P} \left(\frac{T}{T_0}\right)^{1.88} \tag{14}$$

where D_0 is the vapour water diffusion coefficient at pressure P_0 and temperature T_0 ($D_0=21.6\times 10$ -6 m²/s, $P_0=11325$ Pa, $T_0=273.16$ K) [53].

The diffusion coefficient of unsaturated concrete, K_V , is obtained using Eq. (15) by integrating over the pore size range [50]:

$$K_V = \int_{r_c}^{\infty} \frac{k_V}{\tau} \left(\frac{r - t_a}{r}\right)^2 f_d(r) dr \tag{15}$$

where τ is a parameter representing pore tortuosity and it is taken as $\tau = (\pi/2)^2$ [50,54].

As proposed by Ishida et al. [54], the permeability of liquid water can be expressed as a function of moisture flux balance based on the Hagen-Poiseuille equation [54], and the diffusion coefficient of liquid water can be determined as:

$$K_L = \frac{\rho_L}{8\tau^2 \eta} \left(\int_0^{r_c} r f_d(r) dr \right)^2 \tag{16}$$

where ρ_L is the density of liquid water, η is the viscosity of liquid water. For concrete, the convective process at the surface also needs to be considered. Based on the mass balance between ambient air and concrete, the diffusion flux to air can be expressed by Ref. [55]:

$$J = -\frac{D_{va}M_{w}p_{vs}}{RT} \cdot \frac{h_{b} - h_{e}}{\delta}$$
 (17)

where h_b and h_e represent the relative humidity on the concrete surface and the ambient relative humidity, respectively. The parameter δ is the effective thickness of the concrete boundary, which can be taken to be about 25 mm [51].

3.3. Discretization and numerical implementation

The finite element method (FEM) is employed to determine the moisture diffusion in the pore structure by using a specially formulated User Defined Element (UEL) subroutine in Abaqus. In the FEM implementation, $\Omega \subset H^D$ is the domain representing the moisture diffusion region, with D being the space dimension (D = 2) and $\partial\Omega$ representing



Fig. 4. Moisture sorption within a capillary with saturated flow.

the boundary.

Starting from Eq. (8), multiplying by an arbitrary variational field that satisfies the essential boundary conditions δh and integrating over Ω , the following weak form function of the diffusion process can be obtained:

$$\begin{cases}
\frac{\partial h}{\partial t} = \frac{\partial \delta h}{\partial t} \\
\frac{\partial f(h)}{\partial x} = \frac{\partial \delta h}{\partial x} f(h) \\
\int_{\Omega} \left\{ \frac{\partial w}{\partial h} \frac{\partial \delta h}{\partial t} \right\} d\Omega = \int_{\Omega} \left\{ \frac{\partial \delta h}{\partial x} K_{L} \frac{\rho_{L} R T}{M_{W} h} \frac{\partial h}{\partial x} + \frac{\partial \delta h}{\partial x} K_{V} p_{VS} \frac{\partial h}{\partial x} \right\} d\Omega
\end{cases}$$
(18)

To solve Eq. (18), the format of the weak form function is described as:

$$\int_{\Omega} \left\{ \frac{\partial \delta h}{\partial x} K_{L} \frac{\rho_{L} R T}{M_{W} h} \frac{\partial h}{\partial x} + \frac{\partial \delta h}{\partial x} K_{V} p_{VS} \frac{\partial h}{\partial x} - \frac{\partial w}{\partial h} \frac{\partial \delta h}{\partial t} \right\} d\Omega = 0$$
(19)

Taking into account the boundary conditions described in Eq. (17), the Knudsen number is employed to describe the collision between molecules and collision against pore walls of vapour water diffusion, whilst the Hagen-Poiseuille theory is employed to obtain the performance of liquid water diffusion, hence, the adsorption and desorption moisture diffusion function is obtained as follows:

$$\int_{\Omega} \left\{ \frac{\partial \delta h}{\partial x} K_{L} \frac{\rho_{L} R T}{M_{W} h} \frac{\partial h}{\partial x} + \frac{\partial \delta h}{\partial x} K_{V} p_{VS} \frac{\partial h}{\partial x} - \frac{\partial w}{\partial h} \frac{\partial \delta h}{\partial t} \right\} d\Omega
- \int_{\partial \Omega} \delta h \left\{ \frac{D_{va} M_{w} p_{vs}}{R T} \cdot \frac{h - h_{e}}{d} \right\} d\partial \Omega = 0$$
(20)

The Galerkin approach assumes that the variational field, δh , can be expressed by the following function:

$$\delta h = N_T \delta h^N \tag{21}$$

where δh^N is the nodal RH, N_T is the matrix of shape functions derivatives for the scalar fields $(N_T = [N_1, N_2, N_3, N_4])$.

Substituting Eq. (21) into Eq. (20), the following is obtained:

$$\delta h^{N} \left\{ \begin{array}{l} \displaystyle \int_{\Omega} \left\{ \frac{\partial N_{T}}{\partial x} K_{L} \frac{\rho_{L} R T}{M_{W} h} \frac{\partial h}{\partial x} + \frac{\partial N_{T}}{\partial x} K_{V} p_{VS} \frac{\partial h}{\partial x} - \frac{\partial w}{\partial h} \frac{\partial N_{T}}{\partial t} \right\} d\Omega \\ - \int_{\partial \Omega} N_{T} \left\{ \frac{D_{va} M_{w} p_{vs}}{R T} \frac{h - h_{e}}{d} \right\} d\partial \Omega \end{array} \right\} = 0 \tag{22}$$

Since the δh^N is arbitrarily chosen, the weak form function of moisture diffusion can be expressed as:

$$\begin{cases}
\int_{\Omega} \left\{ \frac{\partial N_{T}}{\partial x} K_{L} \frac{\rho_{L} R T}{M_{W} h} \frac{\partial h}{\partial x} + \frac{\partial N_{T}}{\partial x} K_{V} p_{VS} \frac{\partial h}{\partial x} - \frac{\partial w}{\partial h} \frac{\partial N_{T}}{\partial t} \right\} d\Omega \\
- \int_{\partial \Omega} N_{T} \left\{ \frac{D_{va} M_{w} p_{vs}}{R T} \frac{h - h_{e}}{d} \right\} d\partial \Omega
\end{cases} = 0$$
(23)

The discretization of this diffusion system at element level can be described as follows:

$$\begin{cases} \nabla h = B_T h^N \\ \widetilde{h} = N_T \widetilde{h}^N \end{cases} \tag{24}$$

where \tilde{h}^N is nodal incremental relative humidity. B_T is the matrix of shape function derivatives for the tensor fields $(B_T = [\partial N_1/\partial x, \partial N_2/\partial x, \partial N_3/\partial x, \partial N_4/\partial x])$.

Using the Galerkin method [56], the solution equation for FEM can be obtained by combining Eq. (23) and Eq. (24):

$$\int_{\Omega} N_{T}^{T} \frac{\partial h}{\partial t} \frac{\partial w}{\partial h} d\Omega + \int_{\Omega} B_{T}^{T} K_{L} \frac{\rho_{L} R T}{M_{W} h} \frac{\partial h}{\partial x} d\Omega + \int_{\Omega} B_{T}^{T} K_{V} p_{VS} \frac{\partial h}{\partial x} d\Omega
- \int_{\partial \Omega} N_{T}^{T} \frac{D_{Va} M_{w} p_{Vs}}{R T} \frac{(h_{s} - h_{e})}{\delta} dS = 0$$
(25)

A modified Newton-Raphson method is utilized to obtain the

solution for this non-linear diffusion equation [56], which is expressed as:

$$\begin{split} & \left[\int_{\Omega} N_{T}^{T} \frac{N_{T}}{\Delta t} \frac{\partial w}{\partial h} d\Omega + \int_{\Omega} B_{T}^{T} K_{L} \frac{\rho_{L} R T}{M_{W} h} B_{T} d\Omega + \int_{\Omega} B_{T}^{T} K_{V} p_{VS} B_{T} d\Omega \right. \\ & \left. - \int_{\partial \Omega} N_{T}^{T} \frac{\partial v_{u} M_{w} p_{vs}}{R T} \frac{N_{T}}{\delta} dS \right] h^{N} \\ & = \int_{\Omega} N_{T}^{T} \frac{\partial h}{\partial t} \frac{\partial w}{\partial h} d\Omega + \int_{\Omega} B_{T}^{T} K_{L} \frac{\rho_{L} R T}{M_{W} h} \frac{\partial h}{\partial x} d\Omega + \int_{\Omega} B_{T}^{T} K_{V} p_{VS} \frac{\partial h}{\partial x} d\Omega \\ & - \int_{\partial \Omega} N_{T}^{T} \frac{D_{vu} M_{w} p_{vs}}{R T} \frac{(h_{s} - h_{e})}{\delta} dS \end{split} \tag{26}$$

4. Validation of model

4.1. Parameters of model

The model was verified using experimental data by Huang et al. [18]. Prismatic specimens (100 mm \times 150 mm \times 300 mm) (Fig. 5) were cured in a chamber at 23 °C and 100 % RH for 90 days. It was assumed that the hydration process was substantially complete by this stage. After curing, the perimeter of the specimens was sealed and stored in a chamber at 23 °C and 18 % relative humidity for 30 days.

Table 1 shows the R-R pore distribution parameters as obtained by Huang et al. [18], whilst Fig. 6 shows the moisture diffusivity based on the methodology discussed in Section 3.2.

It should be noted that when the pore distribution parameters are not determined experimentally, their values can be estimated as discussed in Section 3.1.

4.2. Comparison between experimental data and simulation results

The RH distribution in the sample can be predicted by the MiMe scale model, introduced above, by using the data and parameters given in Section 4.1. Fig. 5 (b) shows the FEM model developed for the cement matrix, aggregate, and ITZ pore structures; using the method described in Section 2 as well as the initial boundary conditions. The RH evolution in the pore network for the top and bottom 20 mm at different times (i.e., 7, 14 and 30 days) is shown in Fig. 7.

A comparison of the predictions with the experimental data at 30 days is given in Fig. 8. The results overall are in good agreement. However, due to the tortuosity of the pore structure, the RH distribution along the length of the specimen at each depth is not perfectly uniform as for a homogeneous material (see Fig. 9). Fig. 10 (a) shows the RH

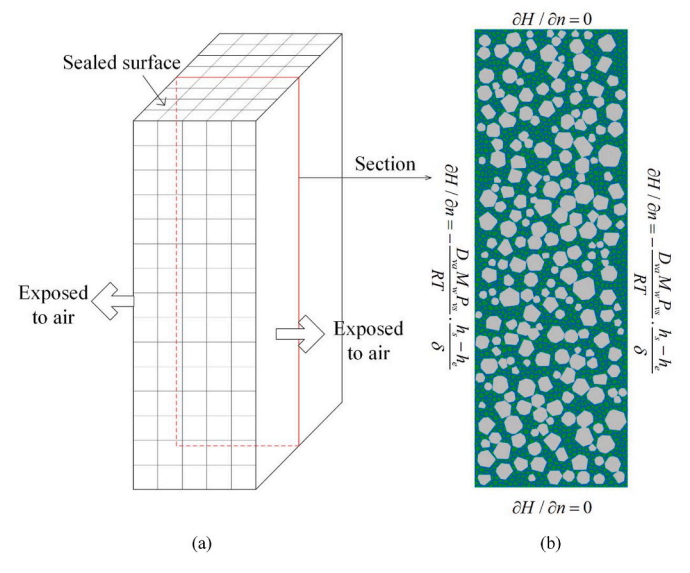
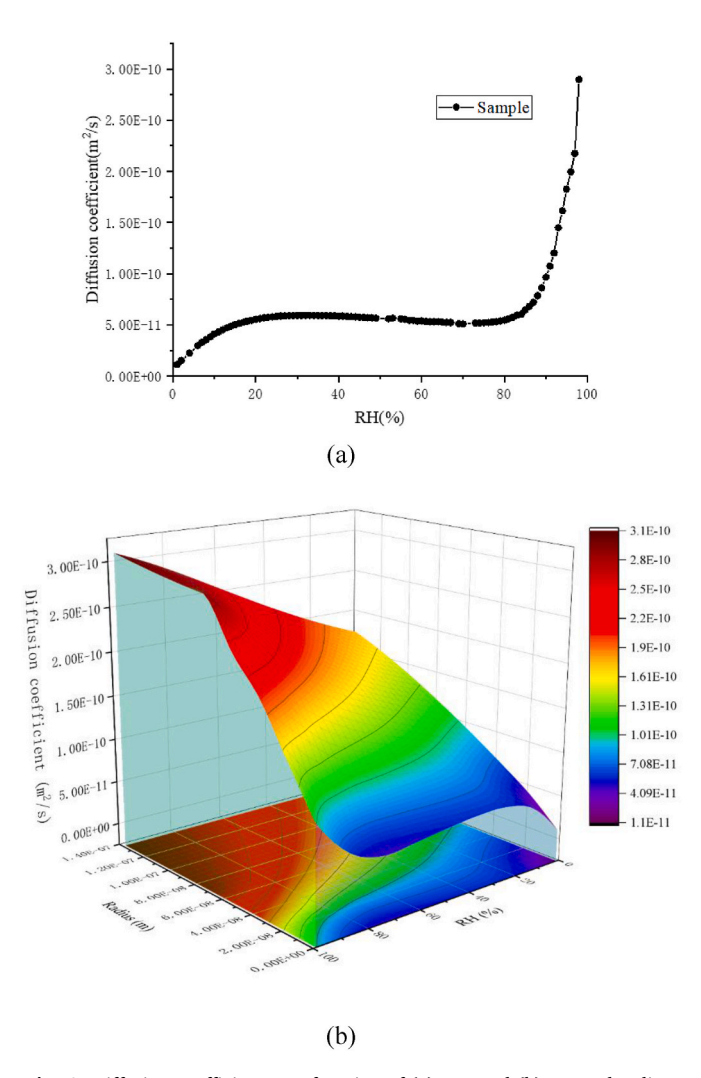


Fig. 5. (a) Sealing conditions of sample, and (b) FEM model of sample.

Table 1Parameters for R-R pore distribution model.

	ϕ_1	B_1 (nm)	ϕ_2	B_2 (nm)	ϕ_3	B_3 (nm)	ϕ_4	B_4 (nm)
Sample	0.042	1.01	0.056	5.00	0.020	32.05	0.012	571.80



 $\textbf{Fig. 6.} \ \ \textbf{Diffusion coefficient as a function of (a) RH, and (b) RH and radius.}$

distribution in the pore structure of the sample, and the variation of RH with depth at five different sections along the length of the specimen. As expected, the RH drops rapidly near the boundaries, but is still almost fully saturated in the middle (98 %).

4.3. Parametric investigation

The effect of ambient relative humidity, temperature and tortuosity on the diffusivity of concrete is shown in Fig. 11(a) and (b) and (c), respectively. The depth of 8 mm is used for these results. As expected, moisture transport increases with a decrease in ambient RH (see Fig. 11 (a)) since this creates a higher flow potential at the concrete-air boundary, increasing the evaporation rate at the concrete surface. The effect of increasing temperature in 20 °C increments is shown in Fig. 11 (b). As the temperature increases, the RH drops faster to a small extent the diffusion ability of concrete [53]. On the contrary, increased tortuosity slows down moisture diffusion by extending the diffusion paths.

The sensitivity of the diffusion model to the main investigated parameters is shown in Fig. 12. In the figure, RH $_{\rm ref}$ is defined as the reference environment characterized by T = 20 °C, RH = 20 % and,

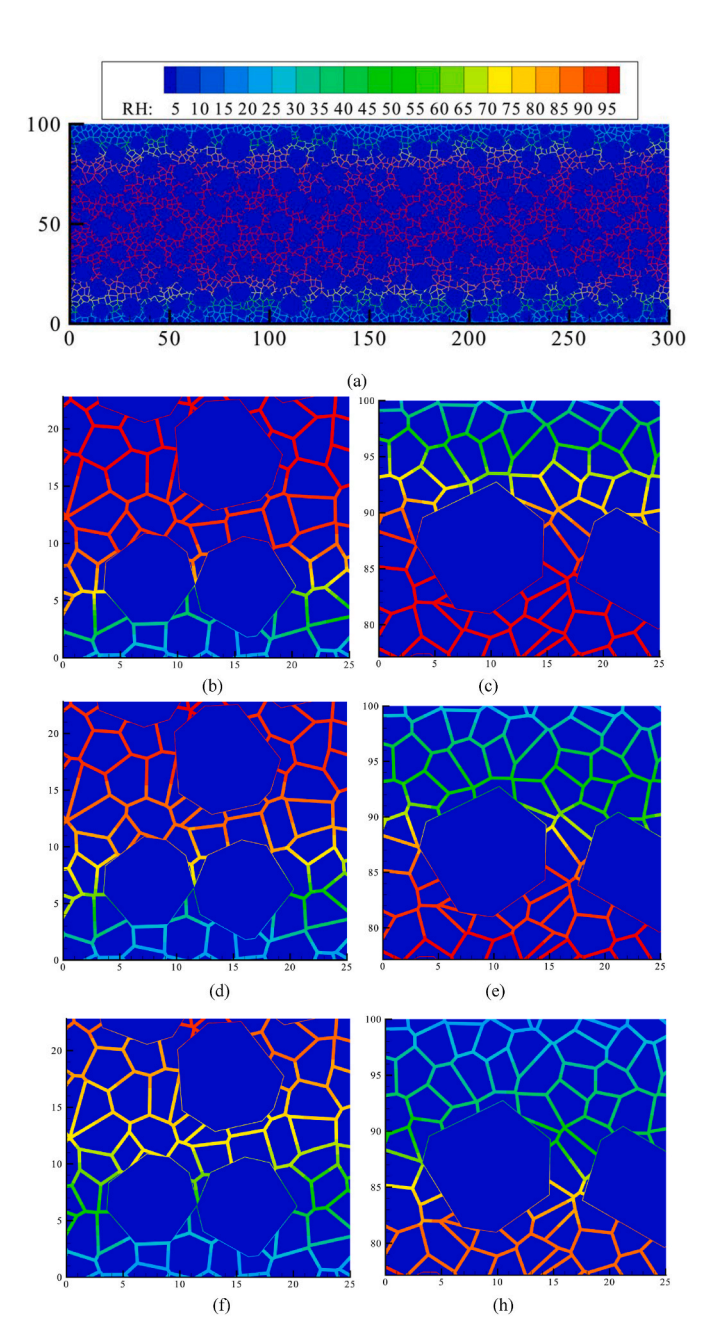


Fig. 7. RH evolution along time, (a) RH distribution at 30th day, (b) Bottom-left corner at 7th day, (c) Top-left corner at 7th day, (d) Bottom-left corner at 14th day, (e) Top-left corner at 14th day, (f) Bottom-left corner at 30th day, and (h) Top-left corner at 30th day.

assuming a tortuosity $\tau=2.5$. The relative change in RH resulting from exposure to different environmental conditions and values of tortuosity is presented. Increasing the temperature by 20 °C or 40 °C, decreases RH by about 3 % and 10.8 %, respectively. Increasing the ambient RH by 20 % or 75 % results in an increase in RH by about 20 % and 50 %, respectively. A change in tortuosity from 2.5 to 2.2 and 2.8, results in changes in RH that vary from -4.8 % and 5.5 %, respectively.

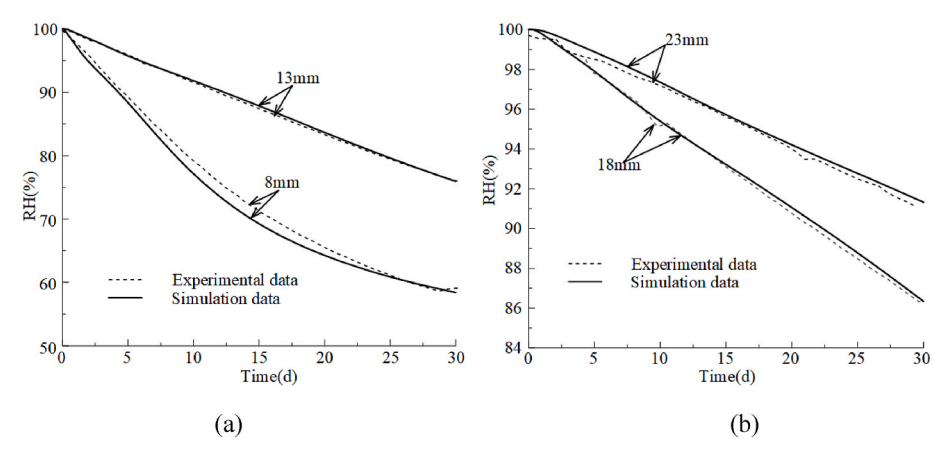


Fig. 8. Comparison between experimental data and simulation results at different depth, (a) 8 mm and 13 mm, and (b) 18 mm and 23 mm.

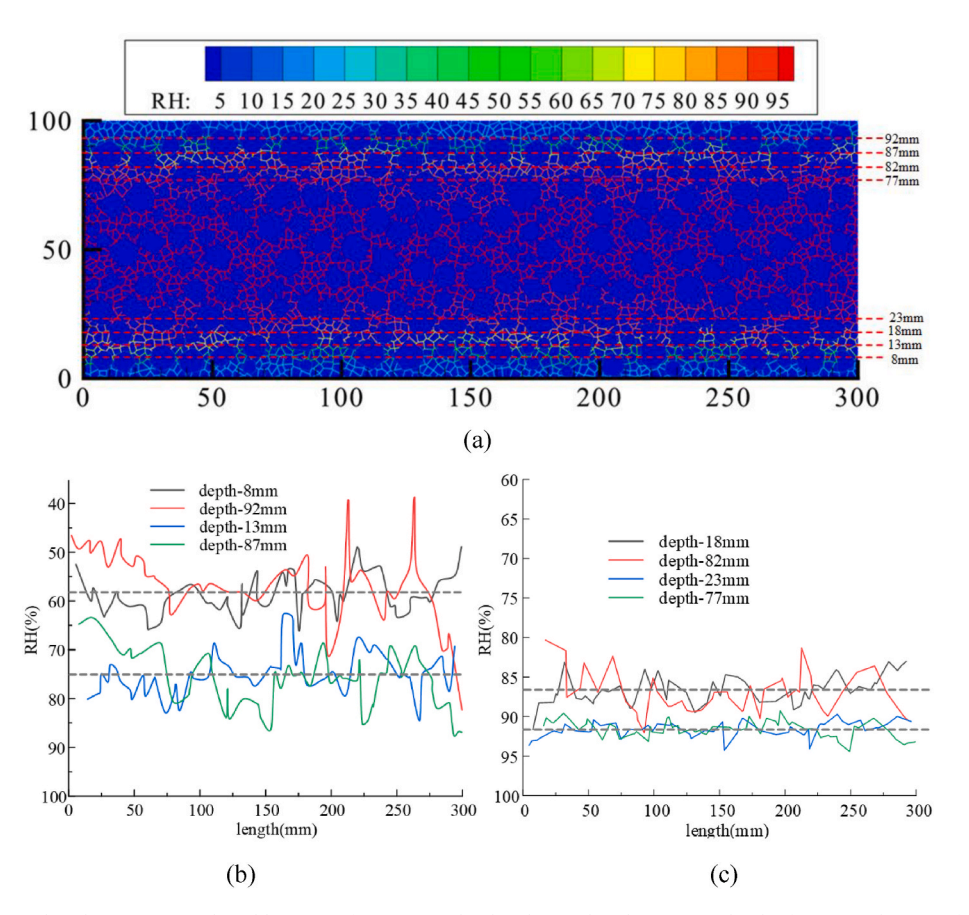


Fig. 9. (a) RH distribution within the pore network and location of measuring depths, (b) RH distribution at a depth of 8 mm and 13 mm from top and bottom, and (c) RH distribution at a depth of 18 mm and 23 mm from top and bottom.

5. Effects of mesostructural features on moisture diffusion

As a typical multi-phase composite material, concrete can be seen as a heterogeneous system with exceedingly complex composite structure at the mesoscopic level. Based on previous models, the important features of concrete are the heterogeneities induced by the addition of coarse aggregate and fine aggregate into the mortar matrix, resulting in the formation of ITZ, and a porous component comprising of mortar. Therefore, the effects of ITZ thickness, fine aggregate content and shape of coarse aggregate are investigated.

5.1. ITZ thickness effect of model

According to previous literature, the ITZ can be modeled as a thin bond layer between aggregate particles and matrix, typically with a thickness ranging from 10 to 50 μm [57]. To investigate the effect of ITZ thickness, thicknesses of 10, 20, 30 and 40 μm are considered. The same distribution, shape and size of aggregate, and pore structure are employed to minimize the effect of other geometric features. It should be noted, however, that the value of the ITZ thickness affects the porosity of the ITZ phase, an in turn the total porosity, albeit slightly, as shown in Table 2. The RH evolution at 8 mm depth with different ITZ thickness is shown in Fig. 13.

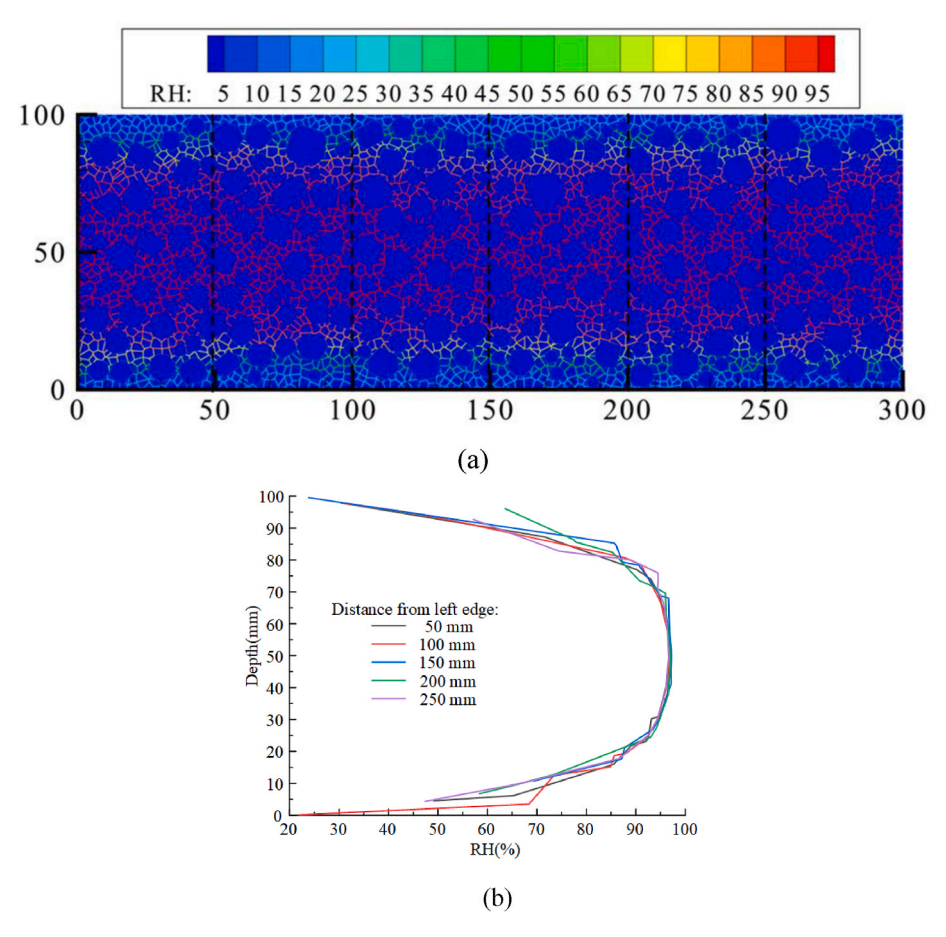


Fig. 10. (a) RH distribution within the pore network and location of measuring sections, and (b) RH distribution along the depth of the sample at different sections.

From Fig. 13, the RH evolution (at 8 mm) slightly increases from 58.4% to 60.3%, which shows that a decrease in ITZ thickness reduces moisture diffusion. This can be attributed to the fact that a decrease in ITZ thickness increases the representative tortuosity of the pore phase, thus decreasing total porosity.

5.2. Fine aggregate effect

To investigate the effect of fine aggregate on moisture diffusion, different volume fractions (3 %, 6 % and 9 %) are considered. As the inclusion of higher volume fractions of fine aggregates would prove computationally costly, and was not deemed to provide any further insights, only these three cases were examined. The resulting aggregate distributions are shown in Fig. 14. The other geometric features, such as volume fraction and distribution of the coarse aggregate and pore structure remain the same. However, the porosity changes slightly with the inclusion of fine aggregate, as shown in Table 3. The RH evolution at 8 mm depth with the different fine aggregate contents is shown in Fig. 15.

From Fig. 15, the RH evolution (at 8 mm) is found to slightly increase, from 58 % to 60 %, with the addition of fine aggregates. This shows that the increase in the volume fraction of fine aggregates slightly reduces the moisture diffusion inside concrete. This results from the decrease in the representative tortuosity of the pore phase, as well as the total porosity of the sample. However, this effect is marginal and, given the high computational costs associated with the generation of the higher number of aggregates, a simplified model only including the coarse aggregated can be adopted.

5.3. Shape effect

To investigate the effect of coarse aggregate shape, two types of aggregate with spherical and ellipsoidal shapes are examined. To minimize the effect of other geometric features, the same pore structure is employed. The models are shown in Fig. 16. The porosity details of different phases are shown in Table 4. The RH evolution at 8 mm depth with different aggregate shapes is shown in Fig. 17.

From Fig. 17, it can be seen that the RH evolution (at 8 mm) changes slightly with different shapes of coarse aggregate, ranging from $58.1\,\%$ for spherical aggregate to $58.4\,\%$ for polygonal aggregate and $58.8\,\%$ for ellipsoidal aggregate. However, again this change is marginal and a correction is needed only if the aggregates are substantially flaky or fibre like

6. Validation of MiMe model

6.1. RH distribution in hardened concrete

The model is verified using experimental data by Jin et al. [58]. One hundred mm cubes were cured in a chamber at $22\pm2\,^\circ\mathrm{C}$ and $95\pm5\,^\circ\mathrm{K}$ RH for 60 days. It was assumed that the hydration process was substantially complete by this stage. After curing, 5 sides of the samples were sealed with epoxy resin while only one side was left exposed. The specimens were subsequently stored in a chamber at 30 $^\circ\mathrm{C}$ and 30 $^\circ\mathrm{K}$ RH and RH measurements inside the concrete at two different depths from the exposed surface (5 mm and 30 mm) were taken for 30 days. Table 5 shows the parameters of the R-R pore distribution model, determined using the procedure described in Section 3.1. The drying moisture diffusion obtained from the implementation of the proposed model for the entire cube is shown in Fig. 18.

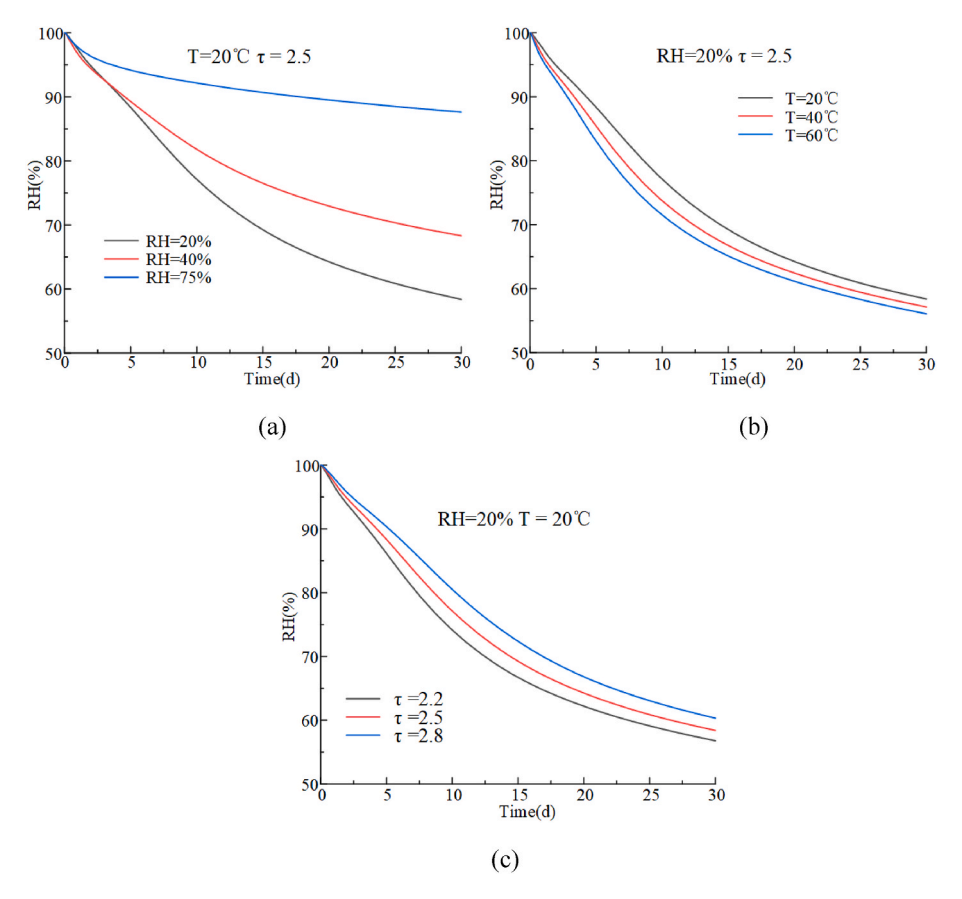


Fig. 11. Effects of parameters on moisture diffusion: (a) Ambient RH, (b) Temperature, and (c) Tortuosity.

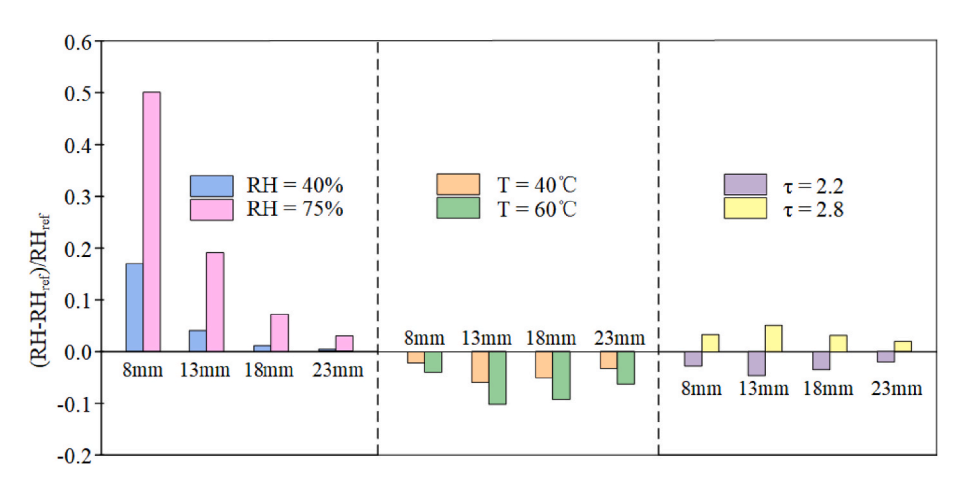


Fig. 12. Sensitivity of RH change to different parameters.

Table 2Porosity for different phases with varying ITZ thickness.

Model	Porosity (%)						
	ITZ	ITZ Pores					
ITZ-50	1.02	11.9	12.92				
ITZ-40	0.82	11.9	12.72				
ITZ-30	0.61	12.0	12.61				
ITZ-20	0.41	12.0	12.41				
ITZ-10	0.2	12.05	12.25				

The RH evolution in the pore network for the top 5 and 30 mm sections is shown in Fig. 19 versus time up to 2800 h. The predictions are overall in good agreement with the experiments, which confirms the ability of MiMe in predicting the RH distribution in hardened concrete.

6.2. RH distribution in early age concrete

The model is further verified for early age concrete using experimental data by Wei et al. [59]. Three beam specimens (1000 mm \times 100 mm \times 38 mm) were cast and sealed completely before being stored in a chamber at a temperature of 23 \pm 2 $^{\circ}$ C and 40 \pm 5 % RH. The specimens were then unsealed from the top surface at different times (7, 28 and 50 days) so as to measure the RH changes induced by self-desiccation and

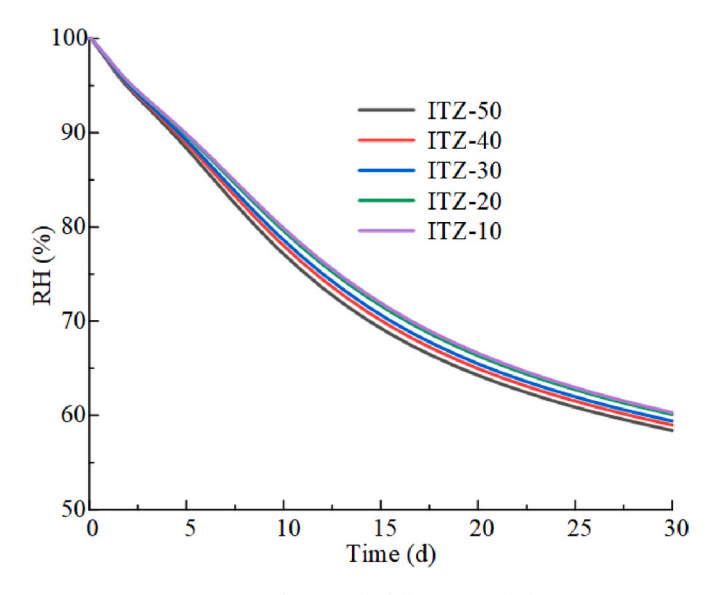


Fig. 13. RH evolution with different ITZ thickness.

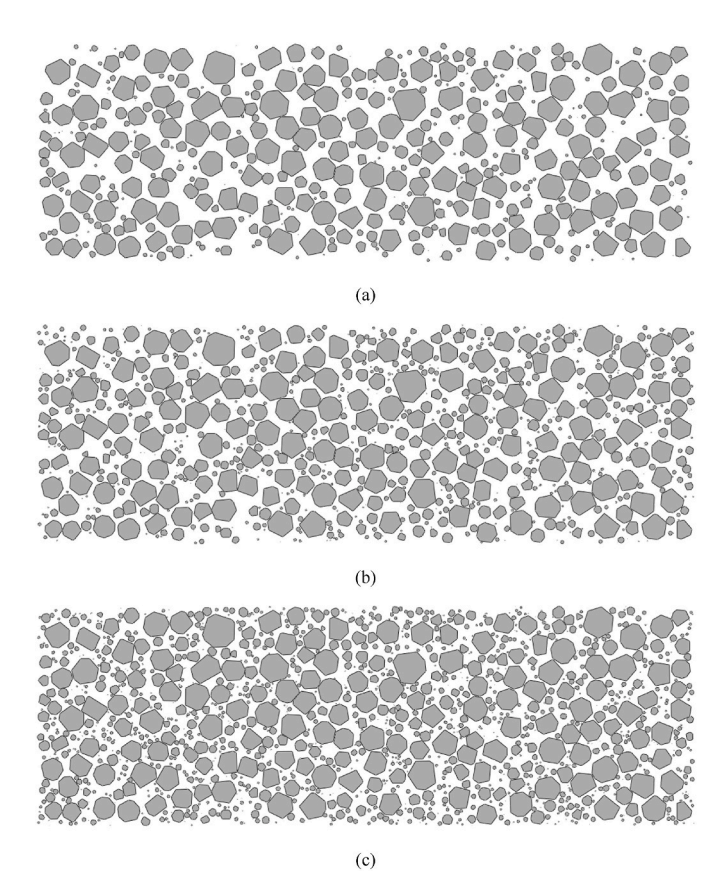


Fig. 14. Distribution of aggregate with different fraction of fine aggregate: (a) 3 %, (b) 6 % and (c) 9 %.

 Table 3

 Porosity for different contents of fine aggregate.

Model	Porosity (%)				
	ITZ	Pores	Total		
Sand-0%	1.02	11.90	12.92		
Sand-3%	1.28	11.27	12.55		
Sand-6%	1.58	10.65	12.23		
Sand-9%	1.93	10.01	11.94		

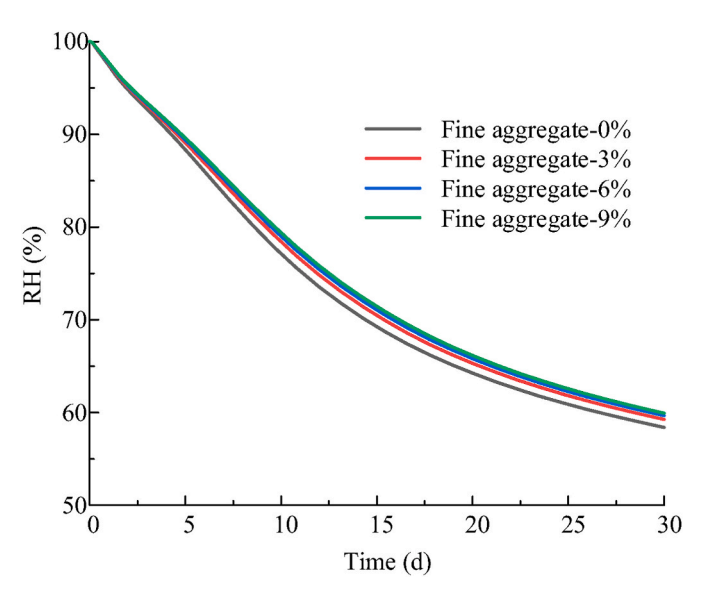


Fig. 15. RH evolution with different fine aggregate fractions.

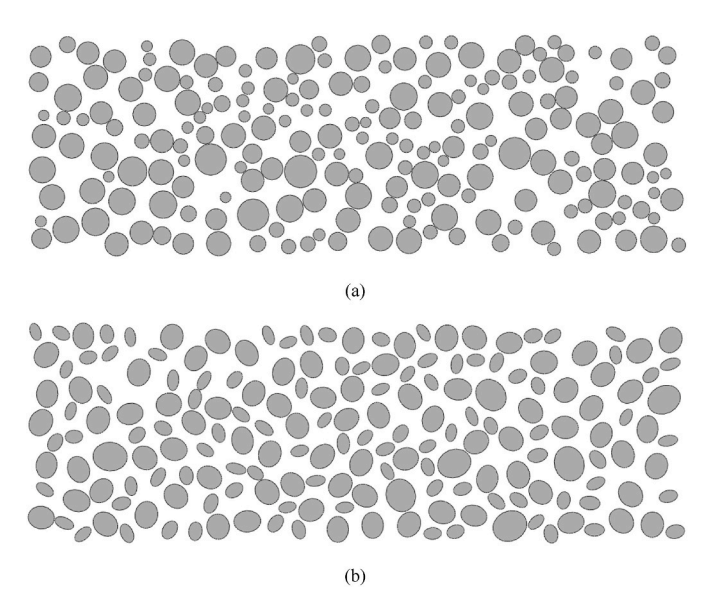


Fig. 16. Distribution of aggregate with different shape of coarse aggregate: (a) spherical aggregate and (b) ellipsoidal aggregate.

 Table 4

 Porosity for different phases with different shape of aggregate.

Model	Porosity (%))	
	ITZ	Pores	Total
Polygonal aggregate	1.02	11.90	12.92
Spherical aggregate	0.91	11.86	12.77
Ellipsoidal aggregate	0.90	11.89	12.79

the drying process. In this sample, the RH change due to self-desiccation is directly obtained from RH evolution of the sealed sample. As for the heat generation during hydration process of small samples, any temperature increase is transient and its effect was ignored in this study.

Table 6 shows the parameters for the R-R pore distribution model determined using the procedure described in Section 3.1. The FEM simulated drying moisture diffusion for the entire beam is shown in Fig. 20.

The RH time history at mid-height (19 mm) is shown for all three

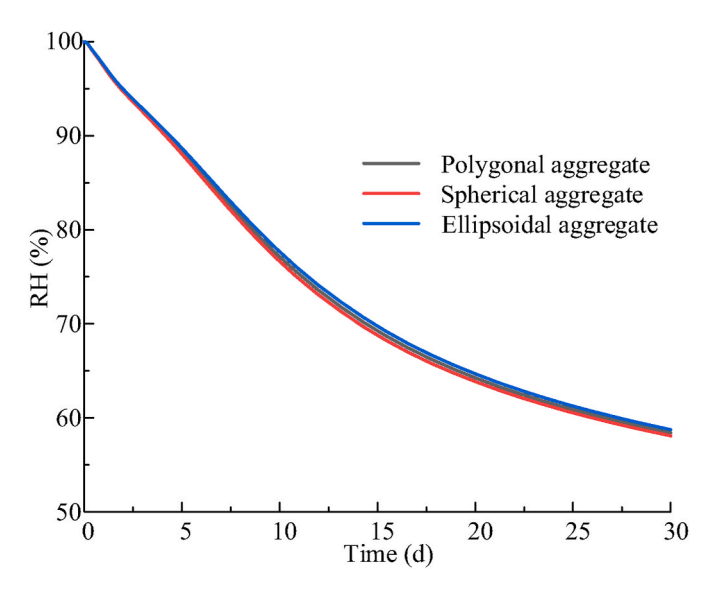


Fig. 17. RH evolution with different shape of coarse aggregate.

beams in Fig. 21. The numerical predictions are in good agreement with the experimental data, confirming the accuracy of MiMe in predicting the RH distribution in early age concrete.

6.3. RH distribution in concrete with different water-cement ratios

The model was further verified using experimental data for concrete with different W/C ratios (0.28, 0.4 and 0.68) by Kim and Lee [60]. Prismatic specimens (100 mm \times 100 mm \times 200 mm) were submerged in water for 3 days. After water-curing, some specimens were exposed to a constant temperature of 20 \pm 1 $^{\circ}$ C and RH 50 \pm 2 %. Fully sealed specimens were also examined to consider the RH evolution of self-desiccation.

Table 7 shows the parameters for the R-R pore distribution model determined using the procedure described in Section 3.1. The FEM simulated drying moisture diffusions for the three prisms are shown in

Fig. 22.

The RH time evolution in the pore network for the top 120 mm up to 60 days is given in Fig. 23. The predictions obtained using the MiMe model are in good agreement with the experimental data, thus confirming the ability of the proposed model to capture the effect of different W/C ratios on RH distribution.

6.4. Accuracy of the simulation results

The average absolute error (AAE) (Eq. (27)) [61] between experimental data and simulation results for the different case studies discussed in the previous sections are summarized in Table 8.

$$AAE = \frac{\sum_{i=1}^{N} \left| \frac{\left| \left(x \right)_{i}^{\text{sim}} - \left(x \right)_{i}^{\text{exp}}}{\left(x \right)_{i}^{\text{exp}}} \right|}{N}$$
(27)

where $(x)_i^{\text{sim}}$ are the simulation results and $(x)_i^{\text{exp}}$ are the experimental values, N is the total number of RH data along with time.

It can be seen that the AAE values for all examined cases are below 2 %, which confirms that the proposed MiMe model can adequately simulate the diffusion and drying process in concrete.

7. Conclusions

To predict moisture diffusion in concrete, a MiMe (micro-meso) model based on Voronoi tessellation and the Monte Carlo method is proposed. The model utilizes a Rayleigh-Ritz (R-R) pore distribution to obtain the diffusion coefficient of concrete, taking into account vapour water diffusion and liquid water permeability. The main conclusions from this study are:

- (1) Using the Monte Carlo method and Voronoi tessellation to generate the geometry and spatial distribution of aggregate, ITZ, and pores, is a viable and flexible method that allows for the tortuosity of concrete to be taken into account directly in the modelling process.
- (2) The correct determination of the diffusion coefficient (vapour and liquid water) and pore size distribution (using the R-R model)

Table 5Parameters for R-R pore distribution model of harden concrete.

	ϕ_1	B_1 (nm)	ϕ_2	B_2 (nm)	ф3	B ₃ (nm)	ф4	B_4 (nm)
PC1	0.0512	0.681	0.0498	2.17	0.0154	11.4	0.0064	571.8
PC2	0.0432	0.657	0.0421	2.01	0.0129	10.2	0.0054	562.4

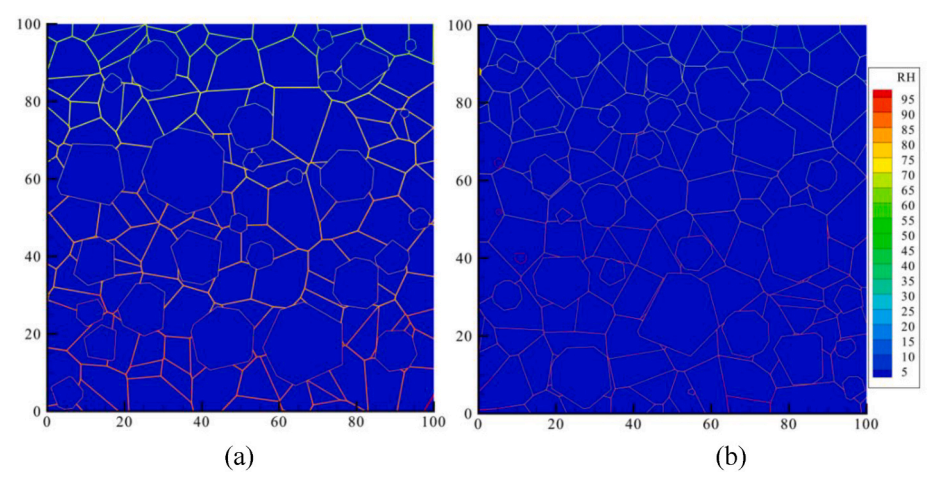


Fig. 18. FEM model for (a) PC1, and (b) PC2 samples.

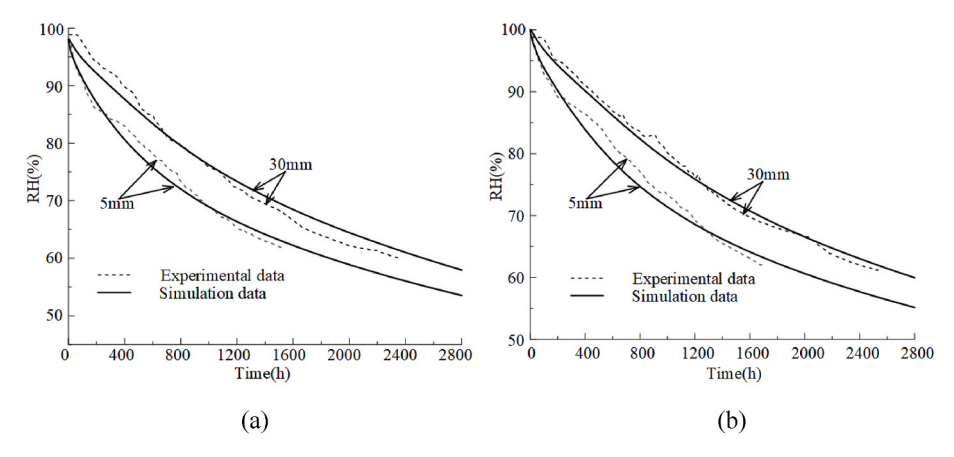


Fig. 19. Comparison between experimental data and simulation results for (a) PC1, and (b) PC2 samples.

Table 6Parameters for R-R pore distribution model of early age concrete.

	ϕ_1	B_1 (nm)	ϕ_2	B_2 (nm)	ϕ_3	B_3 (nm)	ф4	B_4 (nm)
sample	0.04	1.06	0.06	6.32	0.012	73.8	0.008	571.80

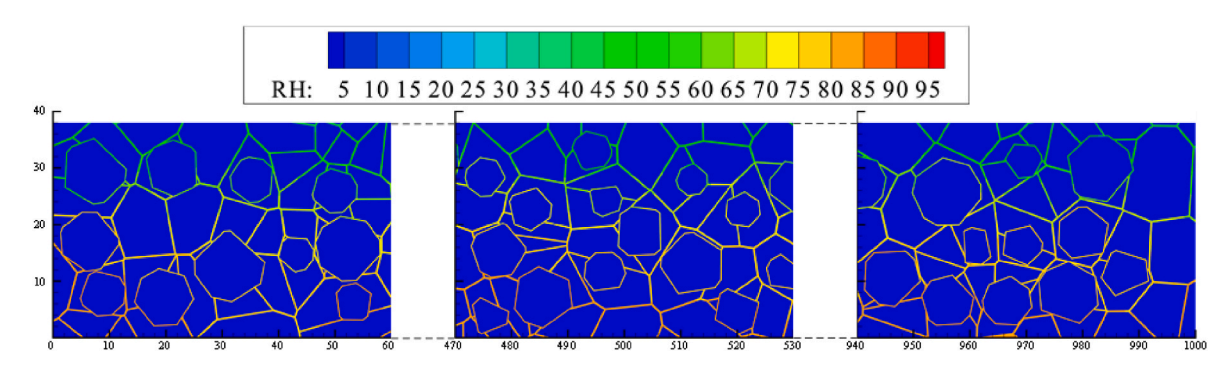


Fig. 20. FEM model for beam sample.

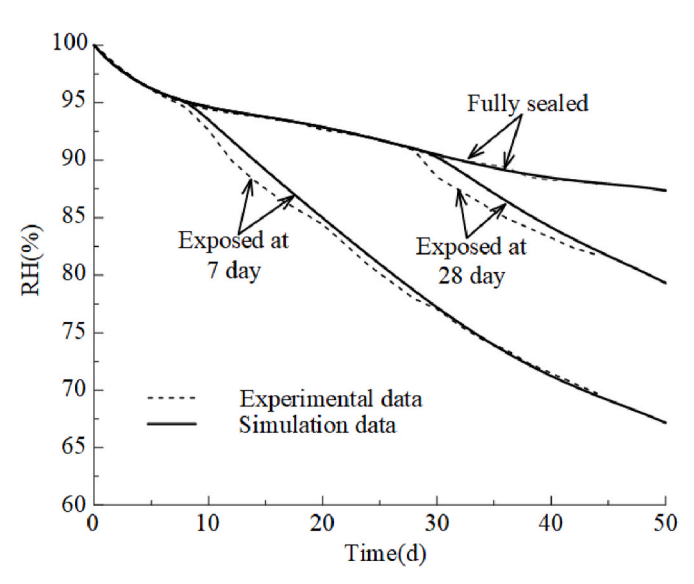


Fig. 21. Comparison between experimental data and simulation results for specimens exposed to unidirectional drying at different ages.

- at the micro level is essential for developing accurate meso-scale models. In the present study moisture diffusion in concrete was described with a maximum error $1.64\ \%$.
- (3) Moisture diffuses faster with increasing ambient temperature (RH diffusion increase from 2 % to 10 %), decreasing RH (RH diffusion increase from 1 % to 50 %), and decreasing tortuosity (RH diffusion increase from −2% to 5 %). The parametric analysis shows that the ambient RH has a more substantial impact on moisture diffusion compared to temperature and tortuosity.
- (4) The RH distribution at a given depth is significantly affected by the assumed tortuosity.
- (5) Moisture diffuses slightly faster with decreasing ITZ thickness and decreasing fine aggregate fractions. The shape of coarse aggregate has a minor effect on moisture diffusion.
- (6) Comparisons of numerical predictions and experimental results show that the RH evolution can be adequately predicted for early age concrete, hardened concrete and concretes with different W/ C ratios.

Integrating the proposed methodology into a fully coupled hygromechanical framework will allow for more accurate predictions of the mechanical behaviour under load. This in turn will enhance the reliability of long-term performance assessments and facilitate the design of

Table 7Parameters for R-R pore distribution model of different W/C concrete.

W/C	ϕ_1	B_1 (nm)	ϕ_2	B_2 (nm)	ϕ_3	B_3 (nm)	ϕ_4	B_4 (nm)
0.28	0.055	0.99	0.036	7.26	0.017	65.2	0.017	551.7
0.4	0.045	1.01	0.04	6.94	0.025	72.1	0.032	553.2
0.68	0.037	1.04	0.05	6.32	0.035	73.8	0.041	557.80

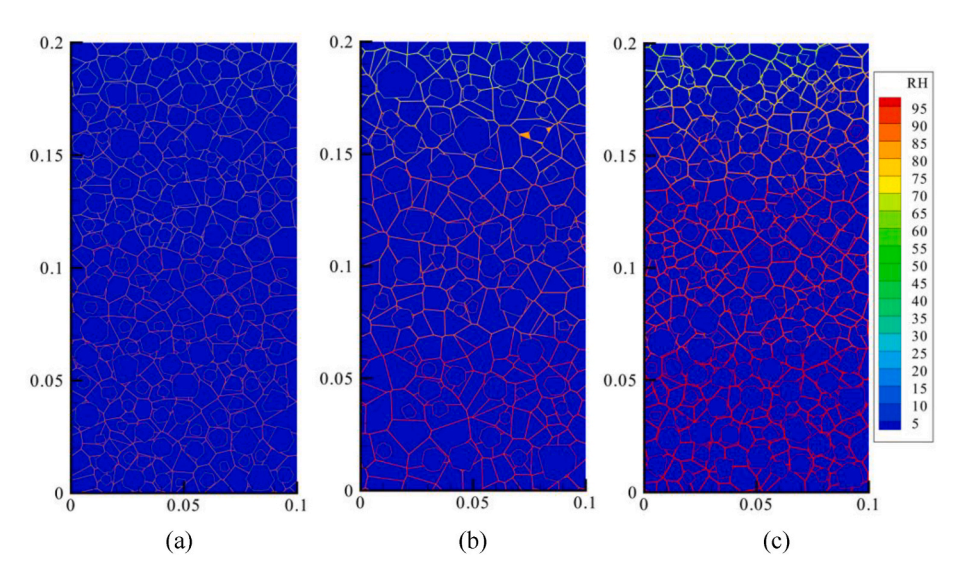


Fig. 22. FEM model for samples with W/C equal to: (a) 0.28, (b) 0.4, and (c) 0.68.

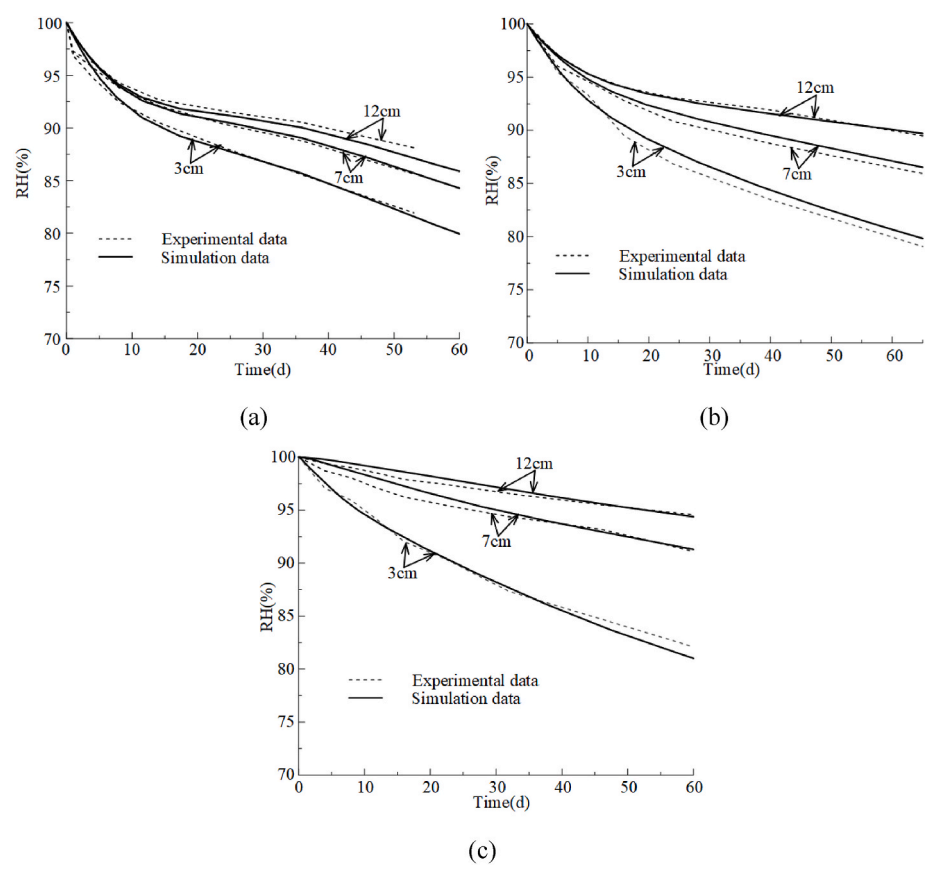


Fig. 23. Comparison between experimental data and numerical predictions for specimens with W/C equal to: (a) 0.28, (b) 0.4, and (c) 0.68.

Table 8AAE between simulation and experiments.

Model	AAE (%) at different depths (mm)									
	5	8	13	18	19	23	30	70	120	
Huang Q [18]	_	1.38	0.27	0.21	_	0.26	-	-	_	
PC1 [43]	1.64	-	-	_	-	-	1.94	-	-	
PC2 [43]	1.56	_	_	_	-	_	1.10	-	_	
Exposed at 7th day [59]	-	-	-	_	0.81	-	-	-	-	
Exposed at 28th day [59]	_	_	_	_	0.66	_	-	_	_	
Full sealed [59]	_	_	_	_	0.25	_	_	_	_	
W/C-0.28 [60]	_	_	_	_	_	_	0.70	0.46	0.61	
W/C-0.4 [60]	_	_	_	_	_	_	0.79	0.49	0.15	
W/C-0.68 [60]	-	-	-	-	-	-	0.59	0.54	0.34	

more durable concrete structures. As shown above, parameters such as shape, size of aggregate and ITZ thickness do not have a significant effect on moisture diffusion. However, it should also be noted that the thickness of the ITZ phase is considered to be uniform in this model and it is not a function of the geometry of the aggregates. In addition, as continuous interconnectivity of the pore structure is assumed, percolating paths are always present and parameters such as the ITZ percolation threshold cannot be directly investigated with this model.

CRediT authorship contribution statement

Songsong Meng: Writing – review & editing, Writing – original draft, Visualization, Validation, Software, Methodology, Formal analysis, Data curation. Yifan Li: Writing – original draft, Visualization, Software, Methodology, Data curation. Iman Hajirasouliha: Writing – review & editing, Writing – original draft, Validation, Supervision. Giacomo Torelli: Validation, Software, Methodology. Maurizio Guadagnini: Writing – review & editing, Writing – original draft, Visualization, Validation, Supervision. Kypros Pilakoutas: Writing – review & editing, Writing – original draft, Visualization, Validation, Supervision, Methodology, Data curation.

Declaration of competing interest

The authors declare that they have no known competing financial interests or personal relationships that could have appeared to influence the work reported in this paper.

Acknowledgments

Giacomo Torelli gratefully acknowledges the financial support provided by the EC (European Commission) through the project SINCERE (grant 101123293, HORIZON-CL5-2022-D4-02), with UK-specific Horizon Europe Guarantee Extension (UKRI grant 10089449). The financial support of the Engineering and Physical Research Council (EPSRC) for the knowledge exchange project 'Predictive thermo-hygral design of concrete for nuclear energy de-risking' is also gratefully acknowledged.

Data availability

Data will be made available on request.

References

- C. Liu, M.Z. Zhang, Microstructure-based modelling of chloride diffusivity in nonsaturated cement paste accounting for capillary and gel pores, Cement Concr. Res. 168 (2023).
- [2] H. Ye, X. Jin, C. Fu, N. Jin, Y. Xu, T. Huang, Chloride penetration in concrete exposed to cyclic drying-wetting and carbonation, Construct. Build. Mater. 112 (2016) 457-463
- [3] X. Zhu, G. Zi, Z. Cao, X. Cheng, Combined effect of carbonation and chloride ingress in concrete, Construct. Build. Mater. 110 (2016) 369–380.
- [4] P. Léger, P. Côté, R. Tinawi, Finite element analysis of concrete swelling due to alkali-aggregate reactions in dams 60 (4) (1996) 601–611.

- [5] S. Multon, A. Sellier, Multi-scale analysis of alkali–silica reaction (ASR): impact of alkali leaching on scale effects affecting expansion tests, Cement Concr. Res. 81 (2016) 122–133.
- [6] L. Basheer, J. Kropp, D.J. Cleland, Assessment of the durability of concrete from its permeation properties: a review 15 (2–3) (2001) 93–103.
- [7] R.R. Hussain, T. Ishida, Development of numerical model for FEM computation of oxygen transport through porous media coupled with micro-cell corrosion model of steel in concrete structures, Comput. Struct. 88 (9–10) (2010) 639–647.
- [8] B. Martin-Pérez, S.J. Pantazopoulou, M.D.A. Thomas, Numerical solution of mass transport equations in concrete structures 79 (13) (2001) 1251–1264.
- [9] E. Samson, J. Marchand, Modeling the transport of ions in unsaturated cement-based materials, Comput. Struct. 85 (23–24) (2007) 1740–1756.
- [10] J.A. Teixeira de Freitas, P.T. Cuong, R. Faria, Hybrid finite elements for nonlinear thermal and hygral problems, Comput. Struct. 182 (2017) 14–25.
- [11] C.Z. Li, X.B. Song, Mesoscale modeling of chloride transport in unsaturated concrete based on Voronoi tessellation, Cement Concr. Res. 161 (2022).
- [12] V. Baroghel-Bouny, M. Mainguy, T. Lassabatere, O. Coussy, Characterization and identification of equilibrium and transfer moisture properties for ordinary and high-performance cementitious materials 29 (8) (1999) 1225–1238.
- [13] G. Mounajed, W. Obeid, A New Coupling FE Model for the Simulation of Thermal-Hydro-Mechanical Behaviour of Concretes at High Temperatures, vol. 37, 2004, pp. 422–432.
- [14] M. Qin, R. Belarbi, A. Aït-Mokhtar, L.O. Nilsson, Coupled heat and moisture transfer in multi-layer building materials, Construct. Build. Mater. 23 (2) (2009) 967–975.
- [15] P.H. Baker, G.H. Galbraith, R.C. McLean, Temperature gradient effects on moisture transport in porous building materials 30 (1) (2009) 37–48.
- [16] S. Caré, E. Hervé, Application of An-phase Model to the Diffusion Coefficient of Chloride in Mortar, vol. 56, 2004, pp. 119–135.
- [17] G. Sun, Y. Zhang, W. Sun, Z. Liu, C. Wang, Multi-scale prediction of the effective chloride diffusion coefficient of concrete, Construct. Build. Mater. 25 (10) (2011) 3820–3831
- [18] Q. Huang, Z. Jiang, X. Gu, W. Zhang, B. Guo, Numerical simulation of moisture transport in concrete based on a pore size distribution model, Cement Concr. Res. 67 (2015) 31–43.
- [19] O.H. Dehwah, Y. Xi, Theoretical Model for the Coupling Effect of Moisture Transport on Chloride Penetration in Concrete, vol. 177, 2024 107431.
- [20] R.M. Christensen, Mechanics of composite materials, Courier Corporation (2012).
- [21] S. Tada, K. Watanabe, Dynamic determination of sorption isotherm of cement based materials, Cement Concr. Res. 35 (12) (2005) 2271–2277.
- [22] M.I. Nizovtsev, S.V. Stankus, A.N. Sterlyagov, V.I. Terekhov, R.A. Khairulin, Determination of moisture diffusivity in porous materials using gamma-method, Int. J. Heat Mass Tran. 51 (17–18) (2008) 4161–4167.
- [23] K. Terheiden, Simultaneous measurement of vapor and liquid moisture transport in porous building materials, Build. Environ. 43 (12) (2008) 2188–2192.
- [24] A. Anderberg, L. Wadsö, Method for simultaneous determination of sorption isotherms and diffusivity of cement-based materials, Cement Concr. Res. 38 (1) (2008) 89–94.
- [25] L.C. Wang, T. Ueda, Meso-scale modeling of chloride diffusion in concrete with consideration of effects of time and temperature 2 (3) (2009) 58–70.
- [26] P. Pipilikaki, M. Beazi-Katsioti, The assessment of porosity and pore size distribution of limestone Portland cement pastes, Construct. Build. Mater. 23 (5) (2009) 1966–1970.
- [27] Y. Zhang, G. Ye, A model for predicting the relative chloride diffusion coefficient in unsaturated cementitious materials, Cement Concr. Res. 115 (2019) 133–144.
- [28] S. Diamond, Mercury porosimetry: an inappropriate method for the measurement of pore size distributions in cement-based materials 30 (10) (2000) 1517–1525.
- [29] H. Ranaivomanana, J. Verdier, A. Sellier, X. Bourbon, Toward a better comprehension and modeling of hysteresis cycles in the water sorption–desorption process for cement based materials, Cement Concr. Res. 41 (8) (2011) 817–827.
- [30] H. Ranaivomanana, J. Verdier, A. Sellier, X. Bourbon, Prediction of relative permeabilities and water vapor diffusion reduction factor for cement-based materials, Cement Concr. Res. 48 (2013) 53–63.
- [31] R.M. Espinosa, L. Franke, Inkbottle Pore-Method: prediction of hygroscopic water content in hardened cement paste at variable climatic conditions, Cement Concr. Res. 36 (10) (2006) 1954–1968.

- [32] N. Pollmann, F. Larsson, K. Runesson, K. Lundgren, K. Zandi, R. Jänicke, Modeling and computational homogenization of chloride diffusion in three-phase meso-scale concrete, Construct. Build. Mater. 271 (2021).
- [33] M. Zhang, G. Ye, K. van Breugel, Modeling of ionic diffusivity in non-saturated cement-based materials using lattice Boltzmann method, Cement Concr. Res. 42 (11) (2012) 1524–1533.
- [34] D. Hou, Y. Jia, J. Yu, P. Wang, Q. Liu, Transport properties of sulfate and chloride ions confined between calcium silicate hydrate surfaces: a molecular dynamics study, J. Phys. Chem. C 122 (49) (2018) 28021–28032.
- [35] P.J. McDonald, V. Rodin, A. Valori, Characterisation of intra- and inter-C-S-H gel pore water in white cement based on an analysis of NMR signal amplitudes as a function of water content, Cement Concr. Res. 40 (12) (2010) 1656–1663.
- [36] R.A. Patel, J. Perko, D. Jacques, G. De Schutter, G. Ye, K. Van Bruegel, Effective diffusivity of cement pastes from virtual microstructures: role of gel porosity and capillary pore percolation, Construct. Build. Mater. 165 (2018) 833–845.
- [37] E.P. Nielsen, M.R. Geiker, Chloride diffusion in partially saturated cementitious material 33 (1) (2003) 133–138.
- [38] E.J. Garboczi, D.P. Bentz, Multiscale analytical/numerical theory of the diffusivity of concrete 8 (2) (1998) 77–88.
- [39] P. Pivonka, C. Hellmich, D. Smith, Microscopic effects on chloride diffusivity of cement pastes—a scale-transition analysis, Cement Concr. Res. 34 (12) (2004) 2251–2260
- [40] B. Bary, S. Béjaoui, Assessment of diffusive and mechanical properties of hardened cement pastes using a multi-coated sphere assemblage model, Cement Concr. Res. 36 (2) (2006) 245–258.
- [41] K. Rajamani, W.T. Pate, D.J. Kinneberg, Time-driven and event-driven Monte Carlo simulations of liquid-liquid dispersions: a comparison 25 (4) (1986) 746–752.
- [42] Q.H. Huang, C.Z. Li, X.B. Song, Spatial distribution characteristics of ellipsoidal coarse aggregates in concrete considering wall effect, Construct. Build. Mater. 327 (2022).
- [43] C. Mora, A. Kwan, H.C. Chan, Particle size distribution analysis of coarse aggregate using digital image processing 28 (6) (1998) 921–932.
- [44] Y. Xia, W. Wu, Y. Yang, X. Fu, Mesoscopic study of concrete with random aggregate model using phase field method, Construct. Build. Mater. 310 (2021).
- [45] A. Delagrave, J. Bigas, J. Ollivier, J. Marchand, M. Pigeon, Influence of the interfacial zone on the chloride diffusivity of mortars 5 (3-4) (1997) 86-92.
- [46] A.E. Idiart, Coupled Analysis of Degradation Processes in Concrete Specimens at the Meso-Level, Universitat Politècnica de Catalunya, 2009.

- [47] N. Damrongwiriyanupap, L. Li, Y. Xi, Coupled diffusion of multi-component chemicals in nonsaturated concrete 11 (3) (2013) 201–222.
- [48] S. Caré, Influence of aggregates on chloride diffusion coefficient into mortar, Cement Concr. Res. 33 (7) (2003) 1021–1028.
- [49] G. Ye, P. Lura, K. van Breugel, Modelling of water permeability in cementitious materials, Mater. Struct. 39 (9) (2006) 877–885.
- [50] K. Maekawa, T. Ishida, T. Kishi, Multi-scale Modeling of Structural Concrete, Crc Press, 2008.
- [51] Y. Xi, Z.P. Bažant, H.M. Jennings, Moisture diffusion in cementitious materials adsorption isotherms 1 (6) (1994) 248–257.
- [52] Y. Mualem, A new model for predicting the hydraulic conductivity of unsaturated porous media, Water Resour. Res. 12 (3) (1976) 513–522.
- [53] D. Quenard, H. Sallee, Water Vapour Adsorption and Transfer in Cement-Based Materials: a Network Simulation, vol. 25, 1992, pp. 515–522.
- [54] T. Ishida, K. Maekawa, T. Kishi, Enhanced modeling of moisture equilibrium and transport in cementitious materials under arbitrary temperature and relative humidity history, Cement Concr. Res. 37 (4) (2007) 565–578.
- [55] D.M. Roy, Water transport in brick, stone and concrete, Cement Concr. Res. 34 (11) (2004).
- [56] T.-T. Nguyen, D. Waldmann, T.Q. Bui, Computational chemo-thermo-mechanical coupling phase-field model for complex fracture induced by early-age shrinkage and hydration heat in cement-based materials, Comput. Methods Appl. Mech. Eng. 348 (2019) 1-28.
- [57] L. Shuguang, L. Qingbin, Method of Meshing ITZ Structure in 3D Meso-Level Finite Element Analysis for Concrete, vol. 93, 2015, pp. 96–106.
- [58] H. Jin, X. Fan, Z. Li, W. Zhang, J. Liu, D. Zhong, L. Tang, An experimental study on the influence of continuous ambient humidity conditions on relative humidity changes, chloride diffusion and microstructure in concrete, J. Build. Eng. 59 (2022).
- [59] Y. Wei, J. Huang, S. Liang, Measurement and modeling concrete creep considering relative humidity effect, Mech. Time-Dependent Mater. 24 (2) (2019) 161–177.
- [60] J.-K. Kim, C.-S. Lee, Moisture diffusion of concrete considering self-desiccation at early ages 29 (12) (1999) 1921–1927.
- [61] G.E. Thermou, I. Hajirasouliha, Design-oriented models for concrete columns confined by steel-reinforced grout jackets, Construct. Build. Mater. 178 (2018) 313–326.